

DECONVOLVING THE HD 81809 BINARY: ROTATIONAL AND ACTIVITY EVIDENCE FOR A SUBGIANT
WITH A SUN-LIKE CYCLE

RICKY EGELAND¹

¹*High Altitude Observatory, National Center for Atmospheric Research, PO Box 3000, Boulder, CO 80307-3000, USA*

ABSTRACT

HD 81809 has one of the highest quality activity cycles from the sample of stars synoptically observed in the Mount Wilson Observatory HK Project. However, this object is in fact a binary system, raising the question as to which of the components is responsible for the observed cyclic activity and what are the properties of that active component. The *Hipparcos* spacecraft obtained resolved two-color photometry for this system that indicates that both components are near the solar temperature. Combined with the precise *Gaia* parallax and empirical bolometric corrections we derive component luminosities of $L_A = 5.8 \pm 0.3 \mathcal{L}_{\odot}^N$ and $L_B = 1.025 \pm 0.055 \mathcal{L}_{\odot}^N$, and radii $R_A = 2.42 \pm 0.08 \mathcal{R}_{\odot}^N$ and $R_B = 1.04 \pm 0.04 \mathcal{R}_{\odot}^N$, confirming that the primary component is a subgiant. We perform an independent estimate of the rotation period of the A component based on $v \sin i$ and find that it agrees with the 40.2 d period previously measured from the Ca HK time series. We explore plausible scenarios for the deconvolved S -index and find that a cycling A component would have an activity level within the bounds of ensemble activity-rotation trends, while a cycling B component likely does not. Based on the available rotation and activity evidence, we find the most likely characterization of the system is a subgiant primary component responsible for the smooth cyclic behavior in Ca HK with $\log(R'_{\text{HK}}) \sim -4.89$, while the secondary component has relatively flat activity at $\log(R'_{\text{HK}}) \sim -5.02$.

Keywords: stars: activity, binaries: spectroscopic, binaries: visual, stars: evolution, stars: solar-type, dynamo

arXiv:1807.10870v2 [astro-ph.SR] 16 Aug 2018

1. INTRODUCTION

Diligent observations of magnetic activity proxies for “Sun-like” stars have enabled astronomers to search for stellar counterparts to the long-studied solar sunspot cycle. Olin C. Wilson and colleagues were the first to commit to such an observation program with the Mount Wilson Observatory (MWO) HK Project using the HKP-1 spectrophotometer (Wilson 1968, 1978). The activity proxy of choice was the emission in the calcium H & K line cores produced in the lower chromosphere by magnetic heating processes (Linsky & Avrett 1970). Wilson’s observational records were extended by the HKP-2 photometer (Vaughan et al. 1978) and after 25 years of observation a variety of activity patterns were discovered in magnetically active stars (Baliunas et al. 1995). Besides the familiar pattern of the quasi-periodic solar cycle (Livingston et al. 2007; Egeland et al. 2017), stars were found with erratic, non-periodic variability or nearly flat activity records. The existence of these varieties of variability raises the question “What are the physical conditions conducive to producing a smoothly varying quasi-periodic magnetic cycle like that of the Sun?”

We can make progress on this question in a statistical sense by carefully analyzing the fundamental properties of a sample of stars whose long-term activity is observed. This is a small sample of at most a few hundred stars at present, due to the difficulty of maintaining such long-term observation programs in a social and scientific environment that prioritises short-term advances. The MWO HK Project endured the longest from 1966–2003. Using 25 years of data for 111 FGK-type stars, (Baliunas et al. 1995) found that about half of their sample had statistically significant evidence for a periodic cycle, about a quarter were erratic variables, and another quarter had flat (or nearly so) activity. The cycling class was further divided into four classes based on their estimated quality: poor, fair, good, and excellent, with the Sun demonstrating an “excellent” cycle. These classes have a noticeably different character, with the “excellent” and “good” classes showing obvious periodicity in their time series like the Sun, while the “fair” and “poor” classes are not so obvious and indeed it is questionable whether they are actually Sun-like cycles at all. For this reason, subsequent studies of the relationship between cycle period and stellar properties such as rotation and convective turnover time typically use only the high-quality “excellent” and “good” cycles (Saar & Brandenburg (1999), Brandenburg et al. (1998), Böhm-Vitense (2007), Brandenburg et al. (2017))

Baliunas et al. (1995) observed that “K-type stars with low $\langle S \rangle$ almost all have pronounced cycles.” But

what about G-type stars, like the Sun? Egeland (2018) conducted a statistical analysis of the (Baliunas et al. 1995) sample, finding that only 3 stars in the G-group ($0.58 \leq (B - V) < 0.75$) have high-quality “excellent” or “good” cycles, including the Sun. The vast majority of the other high-quality cycles (17/21) are from the K-group ($(B - V) \geq 0.75$). The other G-group high-quality cyclers include HD 78366 ($(B - V) = 0.60$) and HD 81809 ($(B - V) = 0.65$). The former has two significant cycle periods and therefore does not have variability qualitatively similar to the Sun, and furthermore is evolved (luminosity class IV-V; Gray et al. (2003)). The latter is the subject of this work; it has a very Sun-like ~ 8 yr “excellent” class cycle, however its characterization is uncertain because it is in fact an unresolved binary system with a convolved $(B - V)$ of 0.65. Because the cycle of the convolved Ca HK signal for HD 81809 is so pronounced, it is clear that the variability is dominated by only one component of the binary. The other component is either flat activity, or has an amplitude of variability in HK flux that is much smaller than the cycling component. In summary, unless the variable component of HD 81809 turns out to be a G-type star, then *there are no other G-type stars in the Baliunas et al. (1995) sample which have a Sun-like cycle.* Egeland (2018) concluded that the Rossby number, the ratio of the rotation period to the convective turnover timescale, appears to be the critical parameter which determines whether a star shall have a Sun-like cycle. The relatively large solar Rossby number is found to be close to that of the K-type stars with high-quality cycles.

HD 81809 was apparently not known to be a binary by Olin Wilson at the onset of the observation program in 1966 (Baliunas et al. 1998), although it has been observed as a visual binary such since at least 1938 (van den Bos 1938; Baize 1985). With only 12 years of data Wilson (1978) found HD 81809 to be the only star with “definitely” cyclic behavior with a period of about 10 years, and remarked that the star is “rather similar to the Sun in spectral type and [cycle] period”. Visual measurements by Baize (1985) found a separation of $\sim 0.4''$, later confirmed with speckle interferometry (McAlister et al. 1990), and an orbital period of 35 yr. Radial velocity measurements by Duquennoy & Mayor (1988) were consistent with the orbital period of 35 yr and component masses of $1.5 \pm 0.5 M_{\odot}$ and $0.8 \pm 0.2 M_{\odot}$. The rotation period measured from the Ca HK time series was found to be quite long, ~ 40 d (Noyes et al. 1984), which led Baliunas et al. (1995) to suggest that the variations were due to the lower-mass component with an estimated spectral type of $\sim K0$. This was motivated by the activity-rotation study of Noyes et al.

(1984), in which such a slow-rotating, moderately active ($\langle S \rangle = 0.172$) star would be peculiar were the higher-mass component (estimated to be $\sim G0V$) responsible for the variability. Later works continued to assume the HK emission of HD 81809 was due to a K-type component with $(B - V) \sim 0.80$ (e.g. Brandenburg et al. 1998; Saar & Brandenburg 1999; Böhm-Vitense 2007). One notable divergence from this interpretation comes from Favata et al. (2008), who studied the X-ray emission of HD 81809 and concluded that only the larger, higher mass component has enough surface area to produce the observed X-ray fluxes assuming solar-like active regions. We will further discuss what we can conclude from the X-ray observations of HD 81809 in Section 6.

The purpose of this work is to use the latest available observations to characterize the components of HD 81809, and from there infer which of the components is most likely responsible for the Ca HK variations resulting in an ~ 8 yr cycle and ~ 40 day rotation. In Section 2 we present the *resolved* two-color photometry from the Tycho instrument on *Hipparcos*, and how these data along with the observed orbital properties update our understanding of the components. Next, in Section 3 we develop an argument based on rotation that suggests the A component is responsible for the Ca HK observations. In Section 4 we attempt to deconvolve the observed S -index based on the resolved $(B - V)$. Finally, we summarize our conclusions in Section 5 and end with a discussion of the implications of our new characterization of HD 81809 in Section 6.

2. OBSERVATIONS AND CHARACTERIZATION OF THE HD 81809 SYSTEM

2.1. Ca II HK Activity Cycle and Rotation

Figure 1 shows the 51-year composite S -index time series for the HD 81809 system, with observations from the MWO HK Project in red and those from the Lowell Observatory Solar-Stellar Spectrograph (SSS) in blue. SSS observations are calibrated to the Mount Wilson scale using a linear regression for near-coincident observations from an ensemble of 26 solar-analog stars and an additional scaling factor to eliminate remaining discontinuity (Egeland 2017). S is defined as:

$$S = \alpha \frac{N_H + N_K}{N_R + N_V} \quad (1)$$

where N_H and N_K are the counts in 1.09 Å triangular bands centered on Ca II H & K in the HKP-2 spectrophotometer, N_R and N_V are 20 Å reference bandpasses in the nearby continuum region, and α is a calibration constant (Vaughan et al. 1978). The binary components are not resolved in these observations, therefore flux in each

of the four bands is convolved. This long time series clearly shows five full and two partial Sun-like cycles. A Lomb-Scargle periodogram analysis (Lomb 1976; Horne & Baliunas 1986) of the composite S -index data finds the cycle period to be 8.17 ± 0.02 yr, where we have estimated the uncertainty using equation (3) of Baliunas et al. (1995), and furthermore have found our cycle period estimate using an additional 25 years of observations to be equivalent to their previous value of 8.17 ± 0.08 . The median activity is $\hat{S} = 0.1751 \pm 0.0003$, where the 1- σ uncertainty is estimated using the median absolute deviation scaled on the assumption of a Gaussian distribution.¹

Donahue (1993) and Donahue et al. (1996) conducted a periodogram analysis on seasonally binned data from MWO available at the time, finding statistically significant periods in 6 of 26 seasons. The mean rotation period Donahue found was 40.2 days with an rms of 2.3 days, and with seasonal measurements ranging from 37.0 to 43.0 days. The maximum difference $\Delta P = 6.0$ days can be interpreted as a sign of differential rotation due to rotational modulations originating from active regions at varied latitudes (Donahue et al. 1996). Donahue (1993) also looked for correlations between seasonal rotation period measurements and seasonal mean activity that could reveal a solar-like pattern of slow rotation at times of low activity when sunspots appear at high latitudes. No such pattern was found for HD 81809. An updated rotation search is planned for HD 81809 and an ensemble of MWO and SSS stars in a future publication. For the present work we will rely on the results of Donahue et al. (1996).

Figure 1 also shows the X-ray 0.2–2.5 keV luminosity timeseries of Orlando et al. (2017) observed by *XMM-Newton* (excluding one high L_X observation presumably due to a flare). The X-ray observations presently cover one whole and two half-cycles, and is clearly in phase with the Ca HK cycle. The median L_X is 3.52×10^{28} erg s⁻¹, and the range is from 1.43 to 8.73×10^{28} erg s⁻¹. (Judge et al. 2003) estimated the solar X-ray flux in the *ROSAT* 0.1–2.4 keV bandpass from *SNOE-SXP* observations, finding it to vary from 6.31×10^{26} to 7.94×10^{27} erg s⁻¹ over the solar cycle with an absolute accuracy of $\pm 50\%$. We estimate the median solar luminosity from this to be the midpoint, 4.29×10^{27} erg s⁻¹. Neglecting the small offset in the bandpass, the median X-ray luminosity of HD 81809 is a factor 8.2 larger than the Sun and the (max – min) amplitude is 10 times larger. A Lomb-Scargle periodogram of the X-ray data finds a

¹ In this work we use \hat{x} to denote median of a series of values x , while the mean is denoted $\langle x \rangle$.

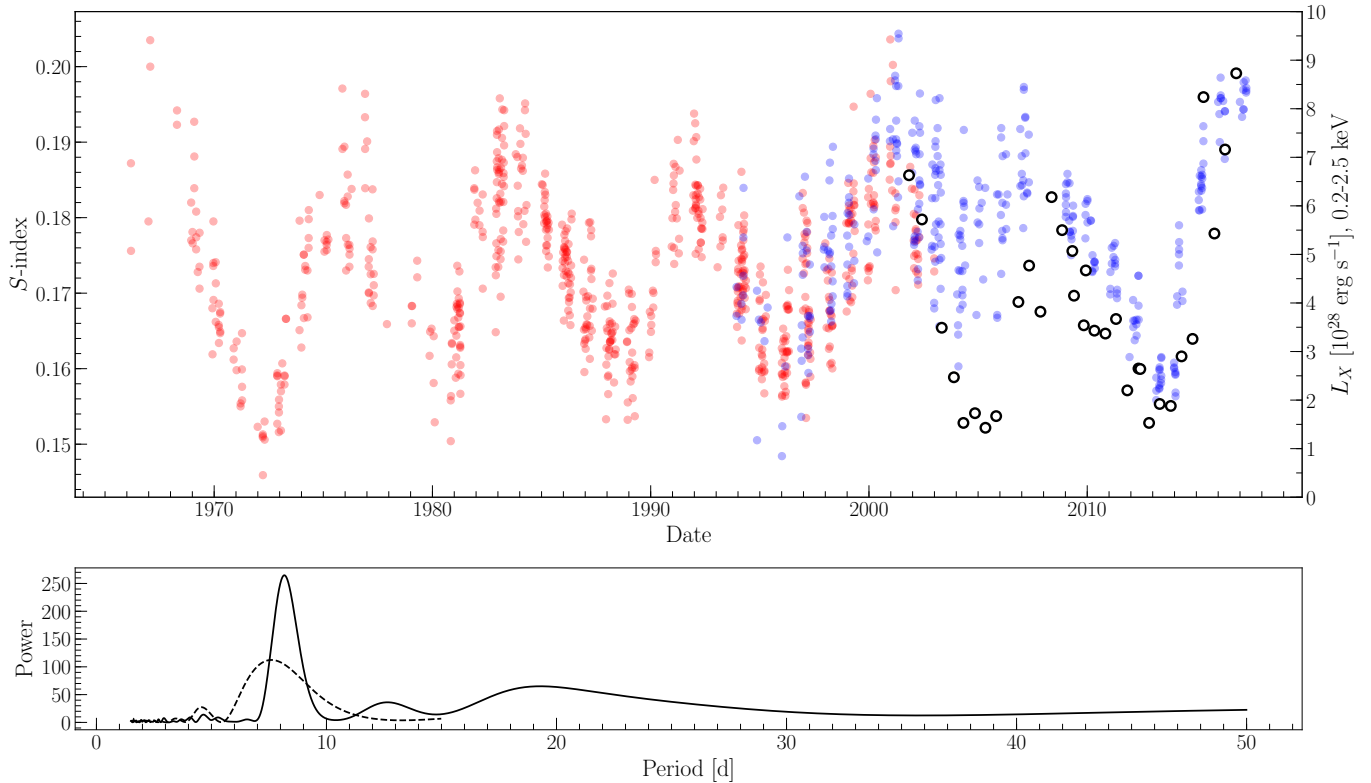


Figure 1. *Top:* Composite S -index time series for HD 81809, with MWO observations in red and SSS in blue. XMM-Newton X-ray observations are overplotted as open circles with the scale on the right axis. *Bottom:* Lomb-Scargle periodogram of the composite S -index time series (solid line) and X-ray observations (dashed line), the latter multiplied by 10 for better visibility.

cycle period of 7.6 ± 0.2 yr. This is notably shorter than the period derived from the S -index time series, which could be due to the cycle covered by the X-ray observations being shorter than the mean. To test this, we computed a Lomb-Scargle periodogram of an S -index time series truncated to within the time limits of the X-ray observations. In that case, we obtained a cycle period of 7.9 ± 0.2 yr, which is compatible to within the uncertainties with the X-ray cycle.²

2.2. Orbit Observations and Component Masses

Table 1 summarizes orbital properties and convolved measurements for the HD 81809 system. We take the latest orbital solution updated using SOAR speckle photometry found in (Tokovinin et al. 2015), in particular the semimajor axis $a = 0.428 \pm 0.001$, orbital period 34.80 ± 0.06 yr, and inclination $i_{\text{orb}} = 85.4 \pm 0.1^\circ$. This solution had a quality grade of 2 out of 5, which is char-

acterized as “Good: most of a revolution, well observed, with sufficient curvature to give considerable confidence in the derived elements. No major changes in the elements likely” (Hartkopf et al. 2001). We adopt the *Gaia* DR2 parallax $\pi = 29.63 \pm 0.76$ mas (Gaia Collaboration et al. 2016, 2018), which agrees to within the uncertainties with the earlier corrected *Hipparcos* parallax from Söderhjelm (1999) ($\pi = 29.0 \pm 1.1$ mas). From this we obtain the mass sum from Kepler’s third law, $M_A + M_B = (a/\pi)^3/P_{\text{orb}}^2 = 2.5 \pm 0.2 M_\odot$. We adopt the radial velocity measurements and resulting mass ratio $q = M_A/M_B = K_1/K_2 = 0.579 \pm 0.084$ of the ninth catalogue of spectroscopic binary orbits³ Pourbaix et al. (2004, hereafter S_{B9}). Combining these values, we obtain component masses $M_A = 1.58 \pm 0.26 M_\odot$ and $M_B = 0.91 \pm 0.15 M_\odot$. These more precise values are consistent to within the uncertainties of the earlier Duquennoy & Mayor (1988) values used by Baliunas et al. (1995) for their interpretations of the binary. However, the best estimate mass of the A component has decreased and that of the B component has increased, placing the latter closer to the solar mass and further

² Orlando et al. (2017) reported an X-ray cycle period of 7.3 ± 0.3 yr by fitting a sinusoid to their data. We were not able to reproduce this result from their published data and using the Lomb-Scargle periodogram. However, by including the presumably flaring observation of 2002-11-02 we obtained a shorter cycle period of 7.2 yr.

³ <http://sb9.astro.ulb.ac.be/DisplayFull.cgi?1474+1>

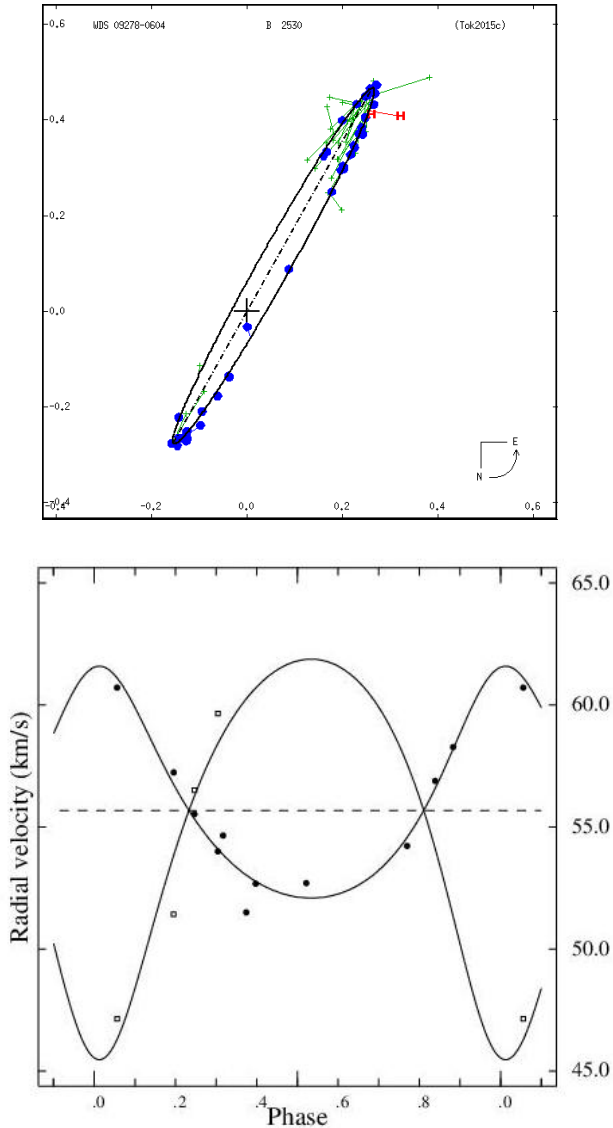


Figure 2. Orbital observations. *Top:* Orbital solution and astrometry from Tokovinin et al. (2015). The position of the primary at the coordinate center is marked by a large cross, the line of nodes is traced by a dash-dotted line, and the orbital solution a solid line. The scale is in arcseconds. Interferometric (solid blue), *Hipparcos* (red), and micrometer (green crosses) measures are connected to their expected positions on the calculated orbit. *Bottom:* Radial velocity observations from S_{B^9} catalog (Pourbaix et al. 2004). Filled circles are the primary and open circles are the secondary. The solid lines show the orbital solution, while the dashed line gives the center-of-mass radial velocity.

from the K-type star that was previously assumed. Unfortunately, the mass uncertainties remain large and are not particularly useful for estimating the expected activity of the components.

Table 1. HD 81809 Orbital and Blended Properties

Property	Value	Reference
parallax, π	29.63 ± 0.76 mas	(1)
semimajor axis, a	0.428 ± 0.001 as	(2)
	14.44 ± 0.37 AU	
orbital period, P_{orb}	34.80 ± 0.06 yr	(2)
orbital inclination, i_{orb}	85.4 ± 0.1 °	(2)
B	6.02	(3)
V	5.38	(3)
$B - V$	0.64	(3)
B_T	6.196 ± 0.014	(4)
V_T	5.483 ± 0.009	(4)
$q = M_A/M_B$	0.579 ± 0.084	(5)
$M_A + M_B$	2.7 ± 0.9	(5)
	2.5 ± 0.2	(E18)
[Fe/H]	-0.29	(6)
$v \sin i$	2.9 ± 0.3 km/s	(7)
rotation period, P_{rot}	40.2 ± 2.3 d	(8)
cycle period, P_{cyc}	8.17 ± 0.02 yr	(E18)
HK activity, \hat{S}	0.1751 ± 0.0003	(E18)
X-ray activity, \widehat{L}_X	3.52×10^{28} erg s $^{-1}$	(9, E18)

References— (1) Gaia DR2 (Gaia Collaboration et al. 2018) (2) Tokovinin et al. (2015) (3) Johnson et al. (1966) (4) Høg et al. (2000) (5) Pourbaix (2000) + S_{B^9} website (6) Holmberg et al. (2009) (7) Ammler-von Eiff & Reiners (2012) (8) Donahue (1993) and Donahue et al. (1996) (9) Orlando et al. (2017) (E18) This work.

2.3. Tycho Photometry and Component Luminosity, Temperature, and Radius

The Tycho Double Star Catalog (TDSC; Fabricius et al. 2002) contains resolved two-color photometry for HD 81809 A & B in the Tycho B_T and V_T bands, which are close to the Johnson B and V bandpasses. TDSC consists of a re-reduction of the Tycho data, whose Tycho-2 catalog (Høg et al. 2000) only contains resolved binary components for separations of $0.8''$ or greater. The double star solution method for TDSC is close to that described in Høg et al. (2000), but in this re-reduction solutions with separations below the previous conservative limit of $0.8''$ were accepted. The smallest accepted separation in TDSC is $0.29''$, while the reported separation for HD 81809 A & B at that epoch

Table 2. HD 81809 Component Properties

Property	A Value	B Value	Reference
H_p	5.746 ± 0.003	7.25 ± 0.01	(1)
B_T	6.34 ± 0.01	8.25 ± 0.02	(2)
	6.17 ± 0.03		
V_T	5.63 ± 0.01	7.52 ± 0.01	(2)
	5.46 ± 0.02		
$(B_T - V_T)$	0.71 ± 0.01	0.73 ± 0.02	(2)
B	6.20 ± 0.01	8.10 ± 0.02	(E18)
	6.02 ± 0.03		
V	5.56 ± 0.01	7.45 ± 0.01	(E18)
	5.38 ± 0.02		
$(B - V)$	0.64 ± 0.01	0.65 ± 0.02	(E18)
	0.64 ± 0.03		
ΔV	1.89 ± 0.02		(E18)
M_V	2.99 ± 0.06	4.88 ± 0.06	(E18)
ΔM_V	2.51 ± 0.06	0.85 ± 0.06	(E18)
T_{eff}	5757 ± 57 K	5705 ± 73 K	(E18)
$L/\mathcal{L}_{\odot}^{\text{N}}$	5.8 ± 0.3	1.025 ± 0.055	(E18)
$R/\mathcal{R}_{\odot}^{\text{N}}$	2.42 ± 0.08	1.04 ± 0.04	(E18)
$M/\mathcal{M}_{\odot}^{\text{N}}$	1.70 ± 0.64	1.00 ± 0.25	(3)
	1.58 ± 0.26	0.91 ± 0.15	(E18)
P_{eq}	42 ± 29	—	(E18)
$\langle P_{\text{rot}} \rangle$	40.2 ± 2.3 d	~ 28 d	(4), (E18)
\hat{S}	~ 0.178	~ 0.157	(E18)
$\log(\widehat{R'_{\text{HK}}})$	~ -4.89	~ -5.02	(E18)

References— (1) [ESA \(1997\)](#) (2) [Fabricius et al. \(2002\)](#) (3) [Pourbaix \(2000\)](#) (4) [Donahue \(1993\)](#) and [Donahue et al. \(1996\)](#) (E18) This work.

NOTE—Values between the A and B columns are the magnitude sums of A and B. ΔM_V is the height above the main sequence as defined by [Wright \(2004\)](#). P_{eq} is the equatorial rotation based on $v \sin i$ and assuming spin-orbit alignment. Values prefixed with \sim are based on the assumed deconvolved activity scenario Case 1 from Section 4.

was $0.52''$. The methods for the photometric solution are described briefly in [Fabricius & Makarov \(2000\)](#) and extensively in [ESA \(1997\)](#). Briefly, the Tycho photometry consists of averaging each slit crossing of the target stars into a global average solution, where each crossing consists of two series of 31 photon counts in the B_T and

V_T bands. The TDSC photometry (B_T , V_T) and color index $B_T - V_T$ for HD 81809 A & B are given in Table 2, as well as their magnitude sums. These magnitude sums may be compared to the *unresolved* Tycho-2 solution of [Høg et al. \(2000\)](#) shown in Table 1 as an internal consistency check. The differences (TDSC - Tycho-2) are $\Delta B_T = -0.025 \pm 0.033$, $\Delta V_T = -0.023 \pm 0.022$, $\Delta(B_T - V_T) = -0.003 \pm 0.040$ indicating they are equivalent to within uncertainties.

We convert the TDSC photometry to the Johnson photometric system (B , V) using the relationships presented in [ESA \(1997\)](#) (Sec 1.3, Appendix 4, Equation 1.3.26). The resulting B , V , and $(B - V)$ are given in Table 2, along with their magnitude sums. As an external consistency check, we compute the magnitude sums to the [Johnson et al. \(1966\)](#) *unresolved* values, obtaining (TDSC - Johnson) differences of $\Delta B = 0.00 \pm 0.01$, $\Delta V = 0.00 \pm 0.01$, and $\Delta(B - V) = 0.00 \pm 0.03$. This *exact* agreement is remarkable given the difficulty of resolving these stars. The resolved color indices are $(B - V)_A = 0.64 \pm 0.01$ and $(B - V)_B = 0.65 \pm 0.02$, both of which are equivalent to within uncertainties to the estimated solar value, $(B - V)_{\odot} = 0.653 \pm 0.003$ ([Ramírez et al. 2012](#)). However, using the system parallax we find that the absolute visual magnitude of the A component, $M_{V,A} = 2.99 \pm 0.06$, is well above the main-sequence, while the B component, $M_{V,B} = 4.88 \pm 0.06$, is close to the solar value, $M_{V,\odot} = 4.83$ ([Allen 1973](#)).

Using the [Flower \(1996\)](#) empirical bolometric corrections and color-temperature relationship (tabulated in [Torres 2010](#)) and the Stephan-Boltzman law we find the fundamental properties for the A component to be $T_{\text{eff},A} = 5731 \pm 47$ K, $L_A/\mathcal{L}_{\odot}^{\text{N}} = 5.8 \pm 0.3$, and $R_A/\mathcal{R}_{\odot}^{\text{N}} = 2.42 \pm 0.08$, where the units are the nominal solar values recommended in IAU 2015 Resolution B3 ([Prša et al. 2016](#)). For the B component, we obtain $T_{\text{eff},B} = 5705 \pm 73$ K, $L_B/\mathcal{L}_{\odot}^{\text{N}} = 1.025 \pm 0.055$, and $R_B/\mathcal{R}_{\odot}^{\text{N}} = 1.04 \pm 0.04$. Here we again find the A component to be evolved and the B component to be nearly identical to the Sun within the uncertainties. However, HD 81809 is relatively metal poor, with $[\text{Fe}/\text{H}] = -0.29$ ([Holmberg et al. 2009](#)).⁴ Assuming the metallicity estimate represents both components, we would expect the metal-poor B component to be less luminous than the Sun if had solar mass and age.

⁴ There are similar estimates from e.g. [Mishenina et al. \(2013\)](#) (-0.28), though some other estimates find even lower metal content, e.g. [Boeche & Grebel \(2016\)](#) (-0.38); [Takeda & Kawonomoto \(2005\)](#) (-0.34). These estimates are based on blended spectra whose flux is dominated by the A component. It is unknown what effect the presence of the B component may have on the metallicity estimates.

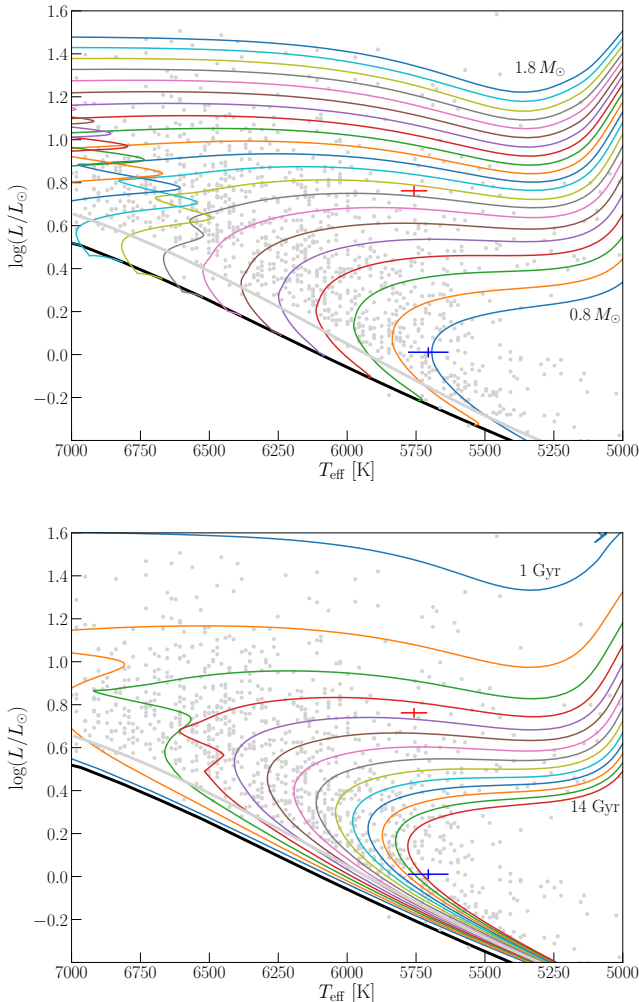


Figure 3. MIST evolutionary tracks and isochrones. *Top:* Colored lines are evolutionary tracks from $0.8 M_{\odot}$ to $1.8 M_{\odot}$ in $0.05 M_{\odot}$ increments with $[\text{Fe}/\text{H}] = -0.29$. The black line is the zero-age main-sequence. HD 81809 A (red) and B (blue) observations are overplotted. Gray points are observations from the GCS with $-0.31 \leq [\text{Fe}/\text{H}] \leq -0.27$, while the gray line is the estimated main-sequence fit to the lower edge of the observations. *Bottom:* Same as above, except that now the colored lines are model isochrones from 1 to 14 Gyr in 1 Gyr increments.

2.4. Comparison with MESA Stellar Evolution Model

Stellar evolution models can help us check for consistency between the the estimated mass (from orbital considerations) and the temperature and luminosity (from photometry). In Figure 3a we show MESA Isochrones & Stellar Tracks (MIST; Choi et al. 2016) evolutionary tracks from $0.8 M_{\odot}$ to $1.8 M_{\odot}$ interpolated to $[\text{Fe}/\text{H}] = -0.29$ using their online tool.⁵ HD 81809 A (red) and

B (blue) are overplotted. The model masses are about $1.18 M_{\odot}$ for the A component and $0.81 M_{\odot}$ for the B component. These are lower than the masses estimated from orbital measurements by 1.5σ and 0.7σ , respectively. Furthermore, the B component appears quite evolved, at the transition to the main-sequence turnoff. This indicates a great age for the B component, which is confirmed the MIST isochrones plotted in Figure 3b, where the indicated age for the B component is over 14 Gyr. This is older than the estimated age of the Universe. Furthermore, A & B do not lie on the same isochrone, as would be expected for a co-evol binary. These issues indicate that there is a serious problem with either the characterization of HD 81809 A & B or the MIST models at this metallicity. To check this, we have plotted a selection of stars from the Geneva-Copenhagen Catalog (GCS; Holmberg et al. 2009) within 0.02 dex of the adopted metallicity. These data reveal that dozens of stars are estimated to be older than 14 Gyr, and furthermore the lower edge of the GCS observations appears to be higher than the model main-sequence. To explore this, we estimate the GCS main-sequence by fitting a third order polynomial to the lowest luminosity stars in 50 K temperature bins (gray line). Comparing this to the MIST model ZAMS, we find a non-uniform difference with an average value in the domain [5300, 7000] K of 0.11 dex in $\log(L)$, or, switching the dependent variable, 207 K in T_{eff} . The difference increases at higher temperatures, which may indicate a scaling issue with the MIST models, or a bias to older stars in the GCS data.

It is beyond the scope of this work to attempt to resolve the difference in the main-sequence position between the MIST models and the GCS observations. We will only note that shifting the model grid by the mean difference 0.11 dex places the A component at ~ 6 Gyr and the B component at ~ 10 Gyr, still about 2σ away from A’s isochrone. A larger shift of about 0.16 dex is required to place A & B on the same ~ 7 Gyr isochrone, however such an alteration places a large number of low-temperature GCS observations below the model main-sequence. Such a deficiency may be in some sense “normal”, as comparisons between MIST and well-characterized eclipsing binaries shows the models are too luminous by ~ 0.2 dex for stars below $\sim 0.7 M_{\odot}$ (see Choi et al. 2016, Section 8.1). However, shifting the grid by 0.17 dex further lowers the model masses to ~ 1.05 and $\sim 0.85 M_{\odot}$ for A & B respectively. This places the mass sum about 1σ below the estimate based on Kepler’s third law.

A systematic underestimate of the HD 81809 metallicity or parallax could also be a factor leading an over-

⁵ <http://waps.cfa.harvard.edu/MIST>

estimate of luminosities with respect to the model grid. Such errors would shift both the A & B components simultaneously, and so as above an ~ 0.16 dex shift would be required to place the components on the same model isochrone. While an error in metallicity would only affect the model masses, a larger parallax would also lower the orbit-based estimate of the component masses so that the model and observations might “meet in the middle.” We find that a parallax of $\sim 35''$ places both components on the same MIST isochrone, however the resulting orbital B mass becomes significantly smaller than the model mass. Finally, errors in the resolved two-color photometry would independently move the A & B components around the HR diagram. From the above analysis of the photometry we are encouraged that the TDSC measurements are both internally and externally consistent with unresolved two-color photometry on the Tycho and Johnson systems, respectively. Furthermore, Fabricius et al. (2002) Figure 8 compares the TDSC photometry to the earlier reduction of Fabricius & Makarov (2000). For bright binaries like HD 81809, both the colors and the component V_T magnitudes are quite consistent. However, as the authors note, when there are differences the TDSC reduction tends to be brighter, more so for the B components. Inspecting Figure 3b, we see that the B component would need $\Delta L \sim -0.2$ dex fainter to lie on the same isochrone as the A component. Using $\Delta M_{\text{bol}} = \Delta L / (-0.4)$, this corresponds to a brightness error of $+0.5$ mag. Using the scatter in Fabricius et al. (2002) Figure 8 as an rough estimate of photometric precision, we can conclude that such a large magnitude error would be very anomalous, but not impossible at the brightness of HD 81809B.

To summarize, when comparing the HD 81809 component positions on the HR-diagram to MIST model isochrones we find issues with the age of the B-component, that it is (1) older than the Universe (2) not the same age as the A-component, and furthermore (3) the model masses are lower than masses estimated from the orbital parameters. Adding GCS stars of the same metallicity to the HR-diagram reveals that there may be a model calibration issue whose resolution by a $+0.11$ dex shift in luminosity may partially resolve issues (1) and (2), while worsening problem (3). A larger shift of $+0.16$ dex is required to fully resolve age issues, while further worsening the mass issue. An error in the measured metallicity would have a similar conflict between model ages and masses versus observations, while a larger parallax could help to resolve most of the issues. Errors in the resolved photometry are still a possibility and may also play a factor. Allowing for the possibility of systematic luminosity calibration error in the model,

the model age for HD 81809 system should be in the range 4–7 Gyr, and the corresponding model mass sum from $2.3\text{--}1.9 M_{\odot}$.

Due to the possibility for MIST model calibration errors, we will put the model results aside and take the observations as they are for the remainder of our analysis.

3. ROTATION-BASED IDENTIFICATION OF THE ACTIVE COMPONENT

Because the cycle shown in Figure 1 is so clean, we assume that the variability is dominated by only one component in the binary. Similarly, we attribute the 40.2 day rotation measurement of (Donahue et al. 1996) to the same active component. We can obtain an independent estimate of rotation period using the projected rotational velocity measured from Doppler broadening, $v \sin i$.

$$\frac{P_{\text{eq}}}{\sin i} = \frac{2\pi R}{v \sin i}, \quad (2)$$

where P_{eq} indicates the rotation period at the stellar equator and R is the radius of the star. We use $v \sin i = 2.9 \pm 0.3 \text{ km s}^{-1}$ from Ammler-von Eiff & Reiners (2012). Next, assuming the rotational axis is aligned with the orbital axis, we use orbital inclination $i = 85.4^\circ \pm 0.1^\circ$ from the binary solution of Tokovinin et al. (2015). This assumption is justified in the work of Hale (1994), who finds that in binary systems with separations $\log(a) \lesssim 1.2$ ($\lesssim 16 \text{ AU}$) the primary component equatorial plane and orbital plane are co-planar to within $\pm 10^\circ$. Using these values and the radius of the A component from above in equation (2) we find $P_{\text{eq,A}} = 42 \pm 29 \text{ d}$. The large uncertainty is dominated by the uncertainty in $v \sin i$, however the best value is close to the measurement of Donahue et al. (1996). Since the Doppler broadening of the blended spectra should be dominated by the much brighter A component ($\Delta m_V = 1.89$ implies a flux ratio $F_A/F_B = 5.70$), and the rotation period from the S -index record agrees with P_{eq} , we conclude that the S -index modulations of HD 81809 are dominated by the evolved A component. Using similar arguments for the B component, we find $P_{\text{eq,B}} = 18 \pm 13 \text{ d}$, such that the angle between the orbital axis and the rotational axis of B would have to be 59° in order for $P_{\text{eq,B}}$ to agree with $P_{\text{rot}} = 40.2 \text{ d}$. Such a large spin-orbit misalignment may be difficult to explain on physical grounds, however see Offner et al. (2016).

Furthermore, the long rotation period attributed to the A component is consistent with our expectations from conservation of angular momentum as an evolved star expands (van Saders & Pinsonneault 2013). Such

a long rotation period for the G-type main-sequence B component is inconsistent with the observational findings of van Saders et al. (2016), who found that rotational braking ceases to operate past a critical Rossby number ($\equiv P_{\text{rot}}/\tau_c$, where τ_c is the convective turnover time; see Noyes et al. 1984) of about 2, thereby temporarily halting the growth of the Rossby number until the star begins evolutionary expansion. If the B component were responsible for the 40.2 d rotational modulations, its Rossby number would be 3.29. The A-component Noyes et al. (1984) Rossby number is similarly large (3.56), however the empirical relationship was developed using main-sequence stars, and is likely invalid for evolved stars (see Gilliland 1985).

4. DECONVOLVING THE S -INDEX

4.1. Mathematical Description

Rewriting the S -index definition (1) for an unresolved binary with components A & B, we have:

$$S_{AB} = \alpha \frac{(N_{H,A} + N_{H,B}) + (N_{K,A} + N_{K,B})}{(N_{R,A} + N_{R,B}) + (N_{V,A} + N_{V,B})}. \quad (3)$$

We now seek to rewrite this in terms of the S indices of the individual components, S_A and S_B . This can be done with some algebra using the definition of the S -index (1) and defining:

$$D \equiv \frac{N_{R,A} + N_{V,A}}{N_{R,B} + N_{V,B}}, \quad (4)$$

resulting with:

$$S_{AB} = \frac{S_B + DS_A}{1 + D}. \quad (5)$$

Notice that D in equation (4) is the ratio of the denominators of the component S -indices, i.e. the photon counts in the two pseudo-continuum bands from the components. In developing an activity index based only on the flux in the H and K bands, Middelkoop (1982) developed a color-correction factor related to the S -index denominator:

$$C_{\text{cf}} \equiv (N_R + N_V)\gamma/f_{\text{bol}}, \quad (6)$$

where $f_{\text{bol}} = \gamma 10^{-0.4(m_V + BC)}$ is the apparent bolometric flux and γ is a constant dependent on extinction. Alternatively, we can relate the flux to the luminosity $f_{\text{bol}} = L/4\pi d^2$, where d is the distance. Then we rewrite D in equation (4) as:

$$D = \frac{L_A}{L_B} \cdot \frac{C_{\text{cf},A}}{C_{\text{cf},B}}. \quad (7)$$

Middelkoop (1982) developed an empirical relation for C_{cf} as a function of $(B - V)$ (see their equation 8), and we have already estimated the component luminosities above. Therefore, D is a known quantity; for HD 81809 its value is 5.80. Now if we can assume a value for one of the component S -indices, then we can use the observed convolved S -index S_{AB} and equation (5) to solve for the other component.

4.2. Estimating Activity of the Flat Component

As discussed above, we assume that only one of the components of HD 81809 is “active” and cycling, while the other has negligible variability, or is a flat-activity star. We can therefore use observations of other flat-activity stars to estimate an S -index for the flat component. While Hall et al. (2007) finds flat-activity stars at a large range of activity levels, most of those above $\log(R'_{\text{HK}}) > -4.75$ were classified as variable in (Baliunas et al. 1995) using longer time series. We therefore use the long ~ 50 -year activity records from the Egeland (2017) sample of solar-analog stars to define a model for flat-activity on the main sequence. The sample is defined by stars with overlapping observation records from both MWO and SSS with effective temperatures within $\sim 5\%$ of the solar value. Starting from the original 27-star sample, we measure the seasonal-median amplitude, defined as $A_s = \max(\hat{S}_i) - \min(\hat{S}_i)$, where \hat{S}_i is the median S -index for season i . We define “low-variability” as any star with A_s lower than the solar value of 0.0203, finding 9 such stars. We define “main-sequence” following Wright (2004) using the absolute magnitude height $\Delta M_V = M_{V,\text{MS}}(B - V) - M_V$ above the *Hipparcos* ensemble mean main sequence, $M_{V,\text{MS}}(B - V)$, defined using the eighth-order polynomial found in the erratum of Wright (2004). Stars with $\Delta M_V < 1$ are considered “main-sequence”, and those with larger ΔM_V are “evolved.” This ΔM_V cut leaves us with 7 stars with effective temperatures within 2% of the solar (and HD 81809 A or B) value. The main-sequence flat-star sample properties are shown in Table 3. The A_s for this sub-sample ranges from 0.0085–0.0178, or 41–87% of the solar variability. The median activity ranges from $\hat{S} = 0.147$ –0.179, with an ensemble median of 0.157 (or $\log(R'_{\text{HK}}) = -5.02$ using $(B - V) = 0.65$). We use this sub-sample ensemble median activity to represent the “typical” activity of a low-variability main-sequence solar-analog star.

Wright (2004) examined the previous suggestions that stars with very low activity ($\log(R'_{\text{HK}}) \leq -5.1$) may be in suppressed activity states analogous to the solar Maunder Minimum. They found that most stars in that activity range were evolved according to the

Table 3. Low-Variability Main-Sequence Stars

HD	T/T_{\odot}^N	R/R_{\odot}^N	L/L_{\odot}^N	ΔM_V	\hat{S}	A_s
43587	1.02	1.24	1.62	0.77	0.1552	0.0111
71148	1.00	1.11	1.24	0.72	0.1567	0.0145
126053	0.98	0.92	0.79	0.22	0.1663	0.0134
141004	1.02	1.38	2.07	0.92	0.1573	0.0178
142373	1.01	1.73	3.06	0.89	0.1470	0.0085
143761	1.00	1.31	1.74	0.71	0.1505	0.0143
176051	1.01	1.20	1.51	0.46	0.1793	0.0157

definition given above. More strictly, they found that *all* such evolved stars had $\log(R'_{\text{HK}}) < -4.9$, while $\log(R'_{\text{HK}}) - 5.1$ is approximately the median activity of evolved stars (see their Figure 3). Therefore, if the evolved A component were the flat-activity component, $\log(R'_{\text{HK}}) \sim -5.1$ is a reasonable estimate for its activity.

In Figure 4 we use equations (5) and (7) along with the component data in Table 2 to model the component S -indices for various assumed activity levels of the flat component. Three scenarios are shown. In Case 1, the luminous subgiant A is the variable component and the flat activity for B is assumed to be $S \sim 0.157$, estimated using the low-variability solar-analog main-sequence sub-sample described above. In Case 2, the main-sequence B component is variable and the subgiant A has an assumed $\log(R'_{\text{HK}}) \sim -5.1$, estimated using the Wright (2004) data. Finally, Case 3 again assumes B is variable and A is flat, but fixes the activity of B to a value of $\log(R'_{\text{HK}}) = -4.85$ that would not be anomalous on the activity-rotation diagram (see below). In the lower panel S is transformed into $\log(R'_{\text{HK}})$ using the formulation of Noyes et al. (1984) and the $B - V$ colors of Table 2. The mean solar activity ($S_{\odot} = 0.1694$; $\log(R'_{\text{HK},\odot}) = -4.9427$) from Egeland et al. (2017) is shown for reference.

Figure 4 shows that when the less-luminous B component is assumed to be flat, as we believe based on the rotational analysis of Section 3, then the activity of the varying component S_A is not much different than that of the original convolved observation regardless of the activity level of the B component. In Case 1, using our assumed $S_B \sim 0.157$, we would find $S_A = 0.178$, slightly more active than the Sun. Converting to R'_{HK} , we have $\log(R'_{\text{HK},B}) \sim -5.02$ implying that $\log(R'_{\text{HK},A}) = -4.89$.

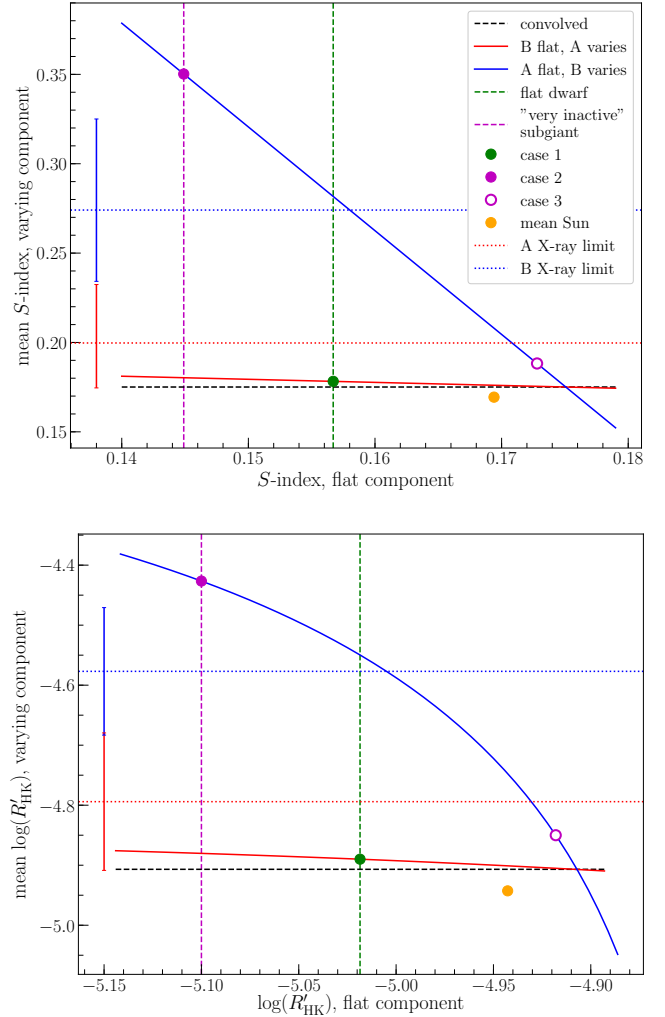


Figure 4. Deconvolving the S -index. *Top:* S -index deconvolution where the x-axis is the assumed activity of the flat component of HD 81809 and the y-axis is the resulting mean activity of the varying component. The convolved S -index is shown as a black dashed line for reference. The red line comes from equation (5) and the assumption that the secondary is flat, while the blue line assumes that the primary is flat. Vertical dashed lines give best estimates for the likely activity of a flat-activity dwarf (green) and subgiant (magenta) respectively. Colored circles give the HD 81809 deconvolved activity cases discussed in the text, with the mean solar activity (orange) plotted for reference. Horizontal dotted lines and associated error bars give an upper limit to activity assuming all of the measured X-ray flux comes from only one component. *Bottom:* Same as above, but using the $\log(R'_{\text{HK}})$ activity index.

Assuming a lower S_B results in nearly negligible increases in S_A , due to the small slope $\Delta S_A/\Delta S_B = 0.172$.

However, if the more-luminous A component is assumed to be flat, the activity of the B component S_B is quite large at the “typical” activity of a sub-

giant. Case 2 assumes $\log(R'_{\text{HK},A}) \sim -5.1$, resulting in $\log(R'_{\text{HK},B}) = -4.43$ (in S , $S_A \sim 0.145$ and $S_B = 0.347$). Significantly higher activity in A would be required to push B into a low-activity regime, which would be required to keep its activity from being anomalous with respect to its rotation (see Figure 5 below). Such a situation is given in Case 3, where we fix the B activity to $\log(R'_{\text{HK}}) \sim -4.85$ and solve for the required activity of A, obtaining $\log(R'_{\text{HK}}) = -4.92$.

4.3. Limits Imposed by X-ray Observations

We used the X-ray/calcium HK relationship described in the appendix of Mamajek & Hillenbrand (2008) to check whether our deconvolved activity levels are compatible with the convolved X-ray observations for HD 81809. We compute upper limits to the expected $\log(R'_{\text{HK}})$ emission by assuming that *all* of the X-ray emission comes from either the A or the B component. Mamajek & Hillenbrand’s relationship is based on $R_X = L_X/L_{\text{bol}}$, which we computed using the data from Table 2. Then, assuming all X-ray emission is from A, we would expect $\log(R'_{\text{HK},A}) \leq -4.79 \pm 0.11$. Similarly for the B component we would expect $\log(R'_{\text{HK},B}) \leq -4.58 \pm 0.11$. The uncertainties given are based purely on the parameter uncertainties of the empirical relationship of Mamajek & Hillenbrand (2008). These upper limits are plotted on Figure 4 along with the deconvolved activity curves and the three special cases described above. The entire activity curve for scenarios in which B is flat and A is the varying component is allowed by the X-ray upper limit, including our best estimate Case 1. For scenarios in which A is flat and B is varying, the X-ray data renders the high-activity portion of the curve unlikely, including Case 2 that assumed the subgiant A component has the typical value from Wright (2004), $\log(R'_{\text{HK}}) = -5.1$. The X-ray data do not fully exclude Case 2, which lies just over 1σ above the upper-limit estimate. Case 3, which is chosen such that the B component does not have an anomalously high activity for a ~ 40 day rotation period (see below), is found to be fully compatible with the X-ray upper limit.

4.4. Comparison to Activity–Rotation Data

We now compare the three scenarios discussed above with an ensemble of stars with known activity and rotation. We use the Mount Wilson sample of 82 stars with rotations from the literature (Egeland 2018) for this purpose. Figure 5 shows the HD 81809 activity scenarios with the MWO ensemble. We see from the figure that for our best estimate of a case where A is varying and B is flat (Case 1) the HD 81809 point falls within the ensemble bounds for activity and rotation. However, for

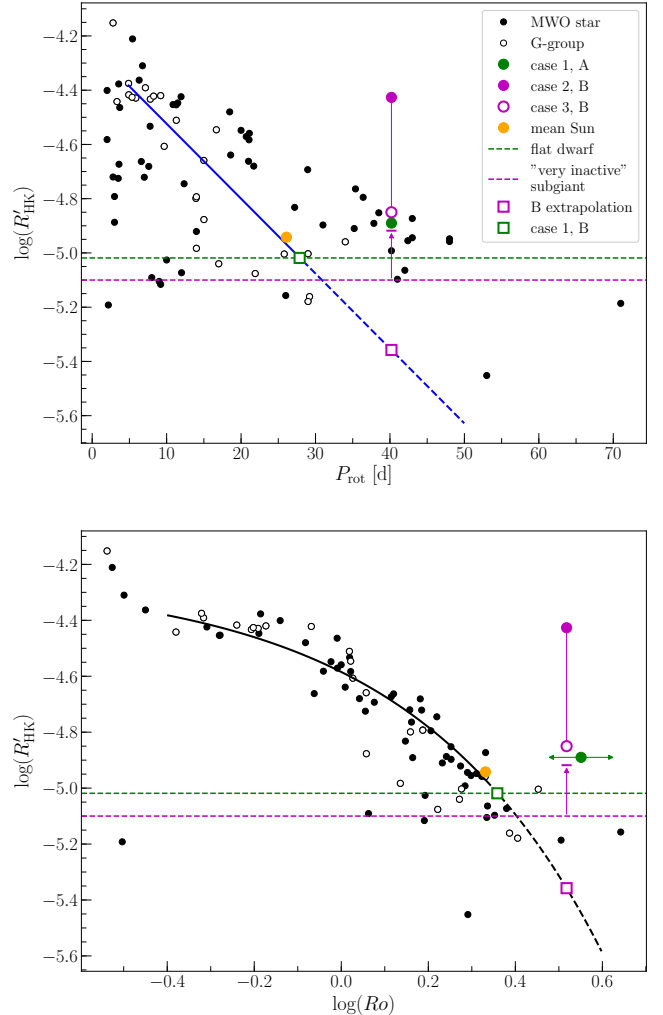


Figure 5. Deconvolved HD 81809 activity-rotation (Top) and activity-Rossby (Bottom) cases from Figure 4 compared to the MWO ensemble with measured rotation periods (black filled circles; G-type stars are open circles). In the top panel, the blue line is the activity-rotation relationship from Mamajek & Hillenbrand (2008) for the B component, while in the bottom panel the general activity-Rossby relationship is shown. In both curves the dashed continuation shows an extrapolation for $\log(R'_{\text{HK}}) < -5.0$ that was not considered in their analysis. The colored circles and lines have the same meaning as in Figure 4, with the addition of the magenta square representing the expected activity level of the B component if it were the “varying” component and also followed the extrapolated Mamajek & Hillenbrand (2008) activity-Rossby relationship, and the green square showing the expected rotation of the B-component given the prototype “flat dwarf” activity level of Case 1. Arrows indicate the directions of possible activity or Rossby number corrections.

our best estimate with B varying and A flat (Case 2), B would be a severe outlier with respect to the ensemble. Case 3 is an upper limit for activity for which a varying B component would *not* be anomalous with respect to the ensemble. In this case, a more active A component is required, as indicated by the magenta arrow. Continuing this trend, it would in fact be possible that the mean activity of a variable B component is *smaller* than a flat A component, which would not necessarily place A as an outlier with respect to the ensemble, since in this case its rotation is unknown and it may be fast enough to avoid being anomalous.

Figure 5 also shows the empirical activity-Rossby number relationship of Mamajek & Hillenbrand (2008) (equation 6). This relationship is based on data with $-5.0 \leq \log(R'_{\text{HK}}) \leq -4.3$, but for illustrative purposes we include the lower-activity extrapolations as dashed lines. In the top panel of Figure 5 the rotation curve specifically refers to the B component ($P_{\text{rot}} = \tau_c \cdot Ro$, where $B - V = 0.65$ results in $\tau_c = 12.2$ days using the relationship of Noyes et al. 1984). The magenta square shows the extrapolated activity level $\log(R'_{\text{HK}}) = -5.36$ if the B component were the varying component with $P_{\text{rot}} = 40.2$ as derived from the Ca HK time series. Such a low activity appears to be unphysical in light of the large ensemble of Figure 6 below. The green square shows the expected rotation period $P_{\text{rot}} \sim 28$ days for the B component under the “flat dwarf” activity scenario of Case 1. This estimate appears to be reasonable by analogy; it is not far below the Sun in parameter space and two other G-type stars have similar activity and rotation measurements. Note that we cannot similarly estimate the expected rotation of the A-component under the Case 2 and Case 3 scenarios because the Mamajek & Hillenbrand (2008) activity-Rossby relationship is valid only for main-sequence stars.

In all cases the computed Rossby number (using Noyes et al. 1984) for the varying component is large with respect to the ensemble. However, if the varying component is A (Case 1), the convective turnover time may in fact be in error due to the evolution (see Gilliland 1985, Figure 10). The estimated effective temperature of the A component lies almost exactly on a transition point in Gilliland’s models, where lower temperatures lead to a steep increase in convective turnover time with respect to the main-sequence value at that temperature, while higher temperatures have a steep relative decrease. Therefore, the correction for A could go either way, as indicated by the green arrows. The B component, on the other hand, is close to the main sequence and so its Rossby number estimation should be as good as any other member of the ensemble. Case 2 would place the

B component activity in a highly anomalous position, while Case 3 would be less so given the large scatter in Rossby number at low activities.

The activity decomposition above does not conclusively decide whether A or B is the varying component. However, the case where A is varying and B is flat results in deconvolved activity levels that are not anomalous with respect to rotation for any reasonable deconvolution scenario. On the contrary, using the best estimate of a mean activity level for a flat subgiant (Case 2) results in an anomalously high activity level for a B component with a ~ 40 d rotation period. If one assumes a higher activity ($\log(R'_{\text{HK}}) > -4.92$) for a flat subgiant A component this problem can be resolved (e.g. Case 3). It remains uncertain whether such an object exists in nature. In the Baliunas et al. (1995) sample, highest activity luminosity class IV or IV-V star classified as “flat” is 31 Aquilae (HD 182572) with $\log(R'_{\text{HK}}) = -5.097$ (Egeland 2018).

4.5. Comparison to Activity–Evolution Data

We examine whether the three activity scenarios derived above are consistent with the observed activity levels from an ensemble of stars at the same point in their evolution as HD 81809 A and B. Following Wright (2004), we compute the height above the *Hipparcos* main sequence ΔM_V for the activity sample of Isaacson & Fischer (2010) with $0.44 \leq (B - V) \leq 0.90$ (1764 stars). The results are shown in Figure 6, which is an updated version of Figure 7 from Wright (2004). Examining Figure 6, we see that for the subgiant A component any of the three cases outlined above is compatible with the ensemble behavior, although there are notably few stars around $\Delta M_{V,A} = 2.51$. However, for the dwarf B component ($\Delta M_{V,B} = 0.85$) Case 1 is the most likely in a statistical sense, while Case 3 is a less likely possibility. Case 2 places the B component in an outlying region which appears to be highly unlikely in the Isaacson & Fischer (2010) ensemble. Both Case 1 and Case 3 place the B component very near to the Sun ($\Delta M_V = 0.83$) in the activity-evolution plane.

4.6. Inclination and Differential Rotation

Donahue et al. (1996) measured seasonal rotation periods for HD 81809 ranging from 37.0 to 43.0 days. Assigning these periods to the A component and using the $v \sin i$ and radius of Table 2, we can estimate some limits on the inclination of the rotation axis, i_{rot} , and the nature of its differential rotation. Recall that assuming spin-orbit alignment we obtained $P_{\text{eq}} = 42 \pm 29$ days. Ignoring for the moment the enormous uncertainty, we can see that if HD 81809A is spin-orbit aligned, then it must

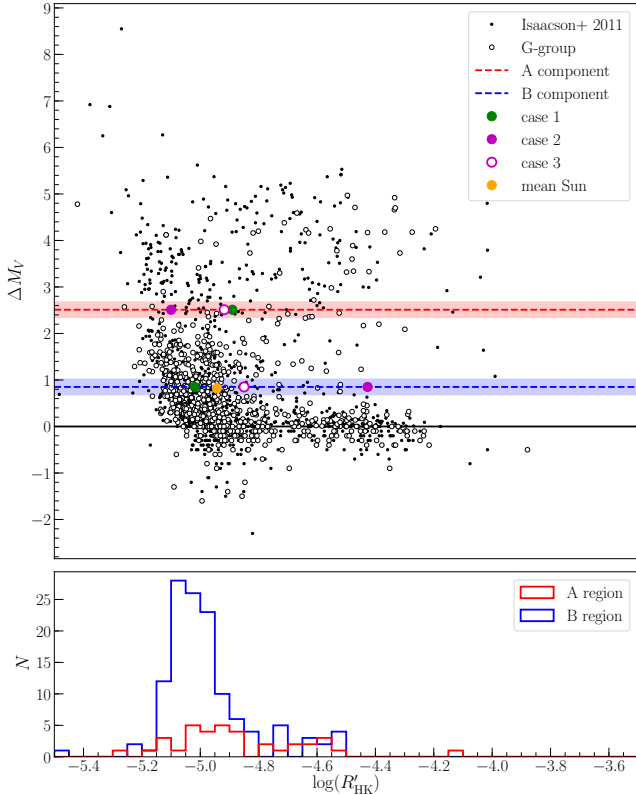


Figure 6. Height above the main sequence ΔM_V versus activity for the catalog of Isaacson & Fischer (2010) with $0.44 \leq (B - V) \leq 0.90$. G-type stars ($0.60 \leq (B - V) \leq 0.70$) are shown as yellow points. The ΔM_V of the A and B components of HD 81809 are indicated with red and blue lines, respectively, with the shaded regions indicating the 3σ uncertainty. The three cases of deconvolved activity given in Figure 4 are shown as colored circles. Histograms of the data contained in the $\pm 3\sigma$ shaded regions are shown in the bottom panel.

have anti-solar or perhaps banded, Jupiter-like differential rotation, as the mean rotation period $P_{\text{rot}} = 40.2$ d is faster than the required equatorial rotation. Conversely, if we assume strict solar-like differential rotation (monotonically increasing rotation period with increasing latitude) and assign the shortest seasonal rotation period to the equator, we find $\sin(i_{\text{rot}}) = 0.88 \pm 0.68$, or $i_{\text{rot}} = 61^\circ \pm 111^\circ$, for a spin-orbit misalignment of $\sim 24^\circ$, significantly larger than the solar misalignment of 7.25° Allen (1973). Given the large (indeed, geometrically impossible) formal uncertainties in the above scenarios no strong conclusions can be drawn. However, there is some reason to suspect that the formal uncertainties in inclination, which are dominated by the uncertainty in the $v \sin i$, are too large. Hale (1994) was able to use similar inclination calculations to find a distribution of spin-orbit misalignments smaller than $\sim 10^\circ$ for binaries

with orbital separations $\lesssim 16$ AU. This result should not have been possible if the inclination uncertainties cover the entire domain $[0^\circ, 90^\circ]$ as in the above case. It also bears noting that many of Hale’s $v \sin i$ measurements had as large or worse relative uncertainty as our adopted $v \sin i$ for HD 81809.

5. CONCLUSIONS

The latest visual (Tokovinin et al. 2015) and radial velocity (Pourbaix et al. 2004) orbital solutions, along with the *Gaia* DR2 parallax for the HD 81809 system indicates component masses of $M_A = 1.58 \pm 0.26 M_\odot$ and $M_B = 0.91 \pm 0.15 M_\odot$. Assuming the Tycho resolved two-color photometry and the *Gaia* parallax are accurate, we conclude that the A component is a subgiant ($T_{\text{eff}} = 5757 \pm 57$ K, $L/L_\odot^N = 5.8 \pm 0.3$), the B component is a main-sequence dwarf ($T_{\text{eff}} = 5705 \pm 73$ K, $L/L_\odot^N = 1.025 \pm 0.055$), and that it is the subgiant A component that is responsible for the well-defined 8.17 yr magnetic activity cycle and 40.2 d rotation period found in archival *convolved* Ca HK observations. The latter conclusion is based on the following lines of evidence:

1. An independent estimate of rotation period using the convolved $v \sin i$ measurement dominated by the larger flux of the A component, along with the A component’s radius, results in a value of ~ 40 d that is consistent with the rotation period measured from the convolved Ca HK observations. Doing a similar exercise for the B component results in disagreement.
2. By assuming a typical value for the Ca HK activity of a flat, main-sequence B component, we derive an activity for the A component that is not anomalous with respect to ensemble activity-rotation data or the expected activity derived from the X-ray flux, while doing the converse and assuming a typical activity for a flat A component results in anomalous activity for the B component (see Figures 4 and 5).
3. The activity scenarios for a cycling B component and flat A component result in atypical activity for the B component with respect to similarly evolved stars (see Figure 6).

Based on analogy with ensemble values, we find $\log(R'_{\text{HK},A}) \sim -4.89$ at $P_{\text{rot},A} = 40.2 \pm 2.3$ d and $\log(R'_{\text{HK},B}) \sim -5.02$ at $P_{\text{rot},B} \sim 28$ d to be a reasonable model for deconvolved activity and rotation. Resolved activity measurements are necessary to characterize the

system with certainty. The Sun-like magnetic activity cycle for a slowly rotating but significantly more luminous star with a Sun-like effective temperature represents a new challenge for dynamo theory.

6. DISCUSSION

Our conclusions depend upon the accuracy of the spatially resolved Tycho two-color photometry as well as the (however reasonable) assumption that the HD 81809A rotation axis is parallel with the orbital axis. The Tycho resolved photometry is near the edge of the instrument’s capability (Fabricius et al. 2002), but the observations are at least consistent with earlier convolved photometry, and the deconvolved activity level for a varying A component is not anomalous with respect to ensemble activity-rotation trends while the contrary case can be. Future data releases from *Gaia* should be able to confirm the color temperature of the HD 81809 components using the G_{RP} and G_{BP} bands of that instrument. However, conclusive evidence of an active A component can only come from resolved spectral observations of an established proxy for magnetic activity. Such observations should be possible with modern telescopes with adaptive optics and favorable conditions.

Our estimated Ca II H & K activity level for the A component is near the middle of the activity distribution for evolved stars with $\Delta M_V > 2$ in Figure 6, while the highest activity evolved flat star in Baliunas et al. (1995) has a lower activity, $\log(R'_{\text{HK}}) = -5.097$. We therefore speculate that perhaps all of the relatively high-activity evolved stars are cycling or otherwise variable, while those with lower activities may indeed be flat. HD 81809A would not be the first cycling subgiant reported. Notably, HD 78366 (G0IV-V) and HD 219834A (G8.5IV) had “good” cycles in the (Baliunas et al. 1995) study, and five other evolved stars had lower-quality cycles reported (Egeland 2018). The quality of the HD 81809 cycle is exceptional, however, and in that regard remarkable for a subgiant. The MWO HK Project began to *purposefully* observe evolved stars in the early 1990s and preliminary results were given in Baliunas et al. (1998). It was shown that the same variety of patterns in long-term variability that exist for main-sequence stars also exist in evolved stars. Unfortunately, the detailed study was never published and observations ceased in 2003. More long-term variability studies are necessary to determine patterns of magnetic activity with evolution. In particular, the widely-used Rossby number formulation of Noyes et al. (1984) likely does not work for evolved stars (Gilliland 1985). A corrected approach may result in reduced scatter in activity-Rossby distributions (e.g. Figure 5) at the low-activity end where

most of the stars are evolved (Wright 2004). Based on the work of Gilliland (1985), it is indeed possible that the Rossby number of HD 81809A is rather close to the solar value, which could make it an unlikely kind of “solar twin” in all the ways which matter to the dynamo (Egeland 2018).

In Section 4.6 we found that if HD 81809A is spin-orbit aligned, then it must have anti-solar or Jupiter-like banded differential rotation, or conversely if it has strictly solar-like differential rotation then it must have a large spin-orbit misalignment of 24° . We caution, however, that these conclusions can only be drawn by ignoring the large formal uncertainties on the derived inclinations, which are primarily due to the large uncertainty in $v \sin i$. A scenario of solar-like differential rotation and large spin-orbit misalignment is contrary to the results of (Hale 1994) that found relatively close binaries (within 16 AU) to be spin-orbit aligned to within $\sim 10^\circ$. We argue that Hale’s result could not have been obtained if the derived inclinations were truly as uncertain as the formal calculations imply. With this point in mind, we find the case for non-solar differential rotation in HD 81809A to be on firmer ground. Such a scenario fits in with the recent proposition of Brandenburg & Gimpapa (2018) who hypothesized that the population of M67 dwarf stars with large Rossby number and relatively high activity may in fact be examples of anti-solar differential rotation, as was predicted by the models of Karak et al. (2015). As we have discussed, HD 81809A also likely has a large Rossby number as well as a high activity compared to other similarly evolved stars.

The HD 81809 system has also been well studied in X-rays (Favata et al. 2004, 2008; Orlando et al. 2017). Favata et al. (2008) assumed solar-like active regions and deduced that the primary component must be emitting most of the flux, because under such an assumption the secondary component would require an unphysical filling factor larger than 1. Radick et al. (2018) did not find this argument convincing, noting that younger, fast-rotating main-sequence stars also have X-ray luminosities well exceeding the Sun’s (e.g. Wright et al. 2011) with a similar surface area. However, the Ca HK and X-ray emission do vary in phase, and therefore it is reasonable to assume that the ~ 40 d rotation period measured in the Ca timeseries also applies to the star responsible for the X-ray cycle. This is certainly *not* the rotation period of a young star, and therefore we believe the intuition of Favata et al. (2004) that the primary is the active component (reaffirmed in Orlando et al. (2017)) was ultimately correct.

Radick et al. (2018) presented 19 years of photometric variability of HD 81809 in the Strömgren b (469 nm,

FWHM 20 nm) and y (548 nm, FWHM 22 nm) bands. It was found that photometric variability is relatively large ($\sigma_{(b+y)/2} = 1.26$ mmag) and the correlation between brightness and Ca HK activity is poor and negative. Compared to their best estimate for the Sun, HD 81809A is 2.6 times more variable in the $(b+y)/2$ bandpass. The filling factors used by Favata et al. (2008) (later reconfirmed by Orlando et al. (2017)) to explain the X-ray luminosities were large; 60% coverage by active regions and 4–40% by brighter “active region cores” from activity minimum to maximum. This was done assuming a radius of $R \sim 2 \mathcal{R}_{\odot}^N$; rescaling to our value of $2.42 \mathcal{R}_{\odot}^N$ these are reduced somewhat to 38% active regions and 2.7–27% by active region cores. Based on our expectation of a correspondence between coronal and photospheric features, we would expect a strong cycle-scale variation in the photometry due to the presence of such structures. Therefore, as pointed out in Radick et al. (2018), that we do not see a clear photometric cycle is puzzling. One possible explanation is that HD 81809A is on the threshold between plage-dominated and spot-dominated photometric variations, such that during times of high activity it is spot-dominated while when activity is low it is plage dominated. Observationally, this corresponds to the region where the change in brightness with change in activity is near zero ($\Delta(b+y)/2/\Delta S \sim 0$). Radick et al. (2018) finds this transition point point at $\log(R'_{\text{HK}}) \sim -4.75$, though there is considerable scatter about the zero-slope line for lower activity (see their Figure 15). Shapiro et al. (2014) used the SATIRE-S irradiance model to predict the possibility of such transition-point stars, which depends on their inclination, in the activity range $-4.9 \leq \log(R'_{\text{HK}}) \leq -4.7$, which is near our estimated activity level for HD 81809A.

It is interesting to consider the magnetic evolution of a star at the estimated mass of HD 81809A. Inspection of Figure 3a shows that HD 81809A was ~ 1000 K warmer ($T_{\text{eff}} \sim 6750$) when it was on the main sequence. This would put it at about the F3 spectral type with $(B-V) = 0.389$ (Pecaut & Mamajek 2013). This is very near the region of the H-R diagram where chromospheric emission (and therefore magnetic activity) begins to be observed for main-sequence stars, presumably coinciding with the onset of a thin outer convective zone (Boehm-Vitense & Dettmann 1980). Such a star is not expected to have strong surface magnetic fields which cause stellar spin-down, therefore it may spend the first 2–4 Gyr (depending on mass) at a relatively fast rotation rate of $P_{\text{rot}} \sim 3\text{--}5$ days (van Saders & Pinsonneault 2013, see Figure 8). The rotation rate then rapidly decreases as expansion takes place, and may reach ~ 40 days in a

fraction of a Gyr (van Saders & Pinsonneault 2013, see Figures 8 and 9)⁶. Thus we now observe HD 81809A during a period of relatively rapid magnetic evolution, as the rotation rate slows and the convection zone expands. The time period for which conditions suitable for a smooth cycle such as HD 81809A now manifests may be remarkably brief with respect to its stellar lifetime. Furthermore, the star was close to magnetically *inert* for its 2–4 Gyr main-sequence lifetime, and likely became progressively more active as expansion produced a thicker convective envelope. Such magnetic evolution is in many ways the opposite as that of the Sun, which began its main-sequence life very magnetically active and then became progressively less so as it spun down over ~ 4 Gyr. The distinctly different magnetic history of HD 81809A and stars in a similar mass range may play a role in the habitability and potential evolutionary history of their respective exoplanets (e.g. Cuntz et al. 2010).

I would like to thank Willie Soon and Jeffrey C. Hall for sharing the S -index data for HD 81809. Thanks also to Phil Judge, Travis Metcalfe, and Scott McIntosh for the useful discussions on this work. Thanks to the anonymous referee for the useful comments which improved the manuscript. This work was funded by the NCAR High Altitude Observatory Newkirk Fellowship and the NCAR Advanced Study Program Postdoctoral Fellowship. The National Center for Atmospheric Research is sponsored by the National Science Foundation.

⁶ As discussed in van Saders & Pinsonneault (2013), subgiant rotation period can serve as a useful diagnostic. From their radius vs. period diagram (Figure 9) we find that the HD 81809A should have a mass $M/M_{\odot}^N \sim 1.2$. The slow rotation then tightly constrains its age to ~ 5 Gyr, according to their age vs. rotation diagram (Figure 8). This radius-rotation based diagnostic is in good agreement with the MIST model mass and age discussed in Section 2.4, but is inconsistent with the estimate based on orbital solutions and parallax..

REFERENCES

- Allen, C. W. 1973, *Astrophysical Quantities*
- Ammler-von Eiff, M., & Reiners, A. 2012, *A&A*, 542, A116
- Baize, P. 1985, *A&AS*, 60, 333
- Baliunas, S. L., Donahue, R. A., Soon, W., & Henry, G. W. 1998, in *Astronomical Society of the Pacific Conference Series*, Vol. 154, *The Tenth Cambridge Workshop on Cool Stars, Stellar Systems and the Sun*, ed. R. A. Donahue & J. A. Bookbinder, 153
- Baliunas, S. L., Donahue, R. A., Soon, W. H., et al. 1995, *ApJ*, 438, 269
- Boeche, C., & Grebel, E. K. 2016, *A&A*, 587, A2
- Boehm-Vitense, E., & Dettmann, T. 1980, *ApJ*, 236, 560
- Böhm-Vitense, E. 2007, *ApJ*, 657, 486
- Brandenburg, A., & Giampapa, M. S. 2018, *ApJL*, 855, L22
- Brandenburg, A., Mathur, S., & Metcalfe, T. S. 2017, *ApJ*, 845, 79
- Brandenburg, A., Saar, S. H., & Turpin, C. R. 1998, *ApJL*, 498, L51
- Choi, J., Dotter, A., Conroy, C., et al. 2016, *ApJ*, 823, 102
- Cuntz, M., Guinan, E. F., & Kurucz, R. L. 2010, in *IAU Symposium*, Vol. 264, *Solar and Stellar Variability: Impact on Earth and Planets*, ed. A. G. Kosovichev, A. H. Andrei, & J.-P. Rozelot, 419–426
- Donahue, R. A. 1993, PhD thesis, New Mexico State University, University Park.
- Donahue, R. A., Saar, S. H., & Baliunas, S. L. 1996, *ApJ*, 466, 384
- Duquenois, A., & Mayor, M. 1988, *A&A*, 195, 129
- Egeland, R. 2017, PhD thesis, Montana State University, Bozeman, Montana, USA
- . 2018, ArXiv e-prints, arXiv:1807.10870, submitted to *ApJ*.
- Egeland, R., Soon, W., Baliunas, S., et al. 2017, *ApJ*, 835, doi:10.3847/1538-4357/835/1/25
- ESA, ed. 1997, *ESA Special Publication*, Vol. 1200, *The HIPPARCOS and TYCHO catalogues. Astrometric and photometric star catalogues derived from the ESA HIPPARCOS Space Astrometry Mission*
- Fabricius, C., Høg, E., Makarov, V. V., et al. 2002, *A&A*, 384, 180
- Fabricius, C., & Makarov, V. V. 2000, *A&A*, 356, 141
- Favata, F., Micela, G., Baliunas, S. L., et al. 2004, *A&A*, 418, L13
- Favata, F., Micela, G., Orlando, S., et al. 2008, *A&A*, 490, 1121
- Flower, P. J. 1996, *ApJ*, 469, 355
- Gaia Collaboration, Prusti, T., de Bruijne, J. H. J., et al. 2016, *A&A*, 595, A1
- Gaia Collaboration, Eyer, L., Rimoldini, L., et al. 2018, ArXiv e-prints, arXiv:1804.09382
- Gilliland, R. L. 1985, *ApJ*, 299, 286
- Gray, R. O., Corbally, C. J., Garrison, R. F., McFadden, M. T., & Robinson, P. E. 2003, *AJ*, 126, 2048
- Hale, A. 1994, *AJ*, 107, 306
- Hall, J. C., Lockwood, G. W., & Skiff, B. A. 2007, *AJ*, 133, 862
- Hartkopf, W. I., Mason, B. D., & Worley, C. E. 2001, *AJ*, 122, 3472
- Høg, E., Fabricius, C., Makarov, V. V., et al. 2000, *A&A*, 355, L27
- Holmberg, J., Nordström, B., & Andersen, J. 2009, *A&A*, 501, 941
- Horne, J. H., & Baliunas, S. L. 1986, *ApJ*, 302, 757
- Isaacson, H., & Fischer, D. 2010, *ApJ*, 725, 875
- Johnson, H. L., Mitchell, R. I., Iriarte, B., & Wisniewski, W. Z. 1966, *Communications of the Lunar and Planetary Laboratory*, 4, 99
- Judge, P. G., Solomon, S. C., & Ayres, T. R. 2003, *ApJ*, 593, 534
- Karak, B. B., Käpylä, P. J., Käpylä, M. J., et al. 2015, *A&A*, 576, A26
- Linsky, J. L., & Avrett, E. H. 1970, *PASP*, 82, 169
- Livingston, W., Wallace, L., White, O. R., & Giampapa, M. S. 2007, *ApJ*, 657, 1137
- Lomb, N. R. 1976, *Ap&SS*, 39, 447
- Mamajek, E. E., & Hillenbrand, L. A. 2008, *ApJ*, 687, 1264
- McAlister, H., Hartkopf, W. I., & Franz, O. G. 1990, *AJ*, 99, 965
- Middelkoop, F. 1982, *A&A*, 107, 31
- Mishenina, T. V., Pignatari, M., Korotin, S. A., et al. 2013, *A&A*, 552, A128
- Noyes, R. W., Hartmann, L. W., Baliunas, S. L., Duncan, D. K., & Vaughan, A. H. 1984, *ApJ*, 279, 763
- Offner, S. S. R., Dunham, M. M., Lee, K. I., Arce, H. G., & Fielding, D. B. 2016, *ApJL*, 827, L11
- Orlando, S., Favata, F., Micela, G., et al. 2017, *A&A*, 605, A19
- Pecaut, M. J., & Mamajek, E. E. 2013, *ApJS*, 208, 9
- Pourbaix, D. 2000, *A&AS*, 145, 215
- Pourbaix, D., Tokovinin, A. A., Batten, A. H., et al. 2004, *A&A*, 424, 727
- Prša, A., Harmanec, P., Torres, G., et al. 2016, *AJ*, 152, 41
- Radick, R. R., Lockwood, G. W., Henry, G. W., Hall, J. C., & Pevtsov, A. A. 2018, *ApJ*, 855, 75
- Ramírez, I., Michel, R., Sefako, R., et al. 2012, *ApJ*, 752, 5
- Saar, S. H., & Brandenburg, A. 1999, *ApJ*, 524, 295

- Shapiro, A. I., Solanki, S. K., Krivova, N. A., et al. 2014, *A&A*, 569, A38
- Söderhjelm, S. 1999, *A&A*, 341, 121
- Takeda, Y., & Kawanomoto, S. 2005, *PASJ*, 57, 45
- Tokovinin, A., Mason, B. D., Hartkopf, W. I., Mendez, R. A., & Horch, E. P. 2015, *AJ*, 150, 50
- Torres, G. 2010, *AJ*, 140, 1158
- van den Bos, W. H. 1938, *Circular of the Union Observatory Johannesburg*, 100, 481
- van Saders, J. L., Ceillier, T., Metcalfe, T. S., et al. 2016, *Nature*, 529, 181
- van Saders, J. L., & Pinsonneault, M. H. 2013, *ApJ*, 776, 67
- Vaughan, A. H., Preston, G. W., & Wilson, O. C. 1978, *PASP*, 90, 267
- Wilson, O. C. 1968, *ApJ*, 153, 221
- . 1978, *ApJ*, 226, 379
- Wright, J. T. 2004, *The Astronomical Journal*, 128, 1273
- Wright, N. J., Drake, J. J., Mamajek, E. E., & Henry, G. W. 2011, *ApJ*, 743, 48